# Bond Flexing, Twisting, Anharmonicity and Responsivity for the IR-active modes of Benzene

**Yong Yang, Tianlv Xu, Steven R. Kirk* and Samantha Jenkins***

*Key Laboratory of Chemical Biology and Traditional Chinese Medicine Research and Key Laboratory of Resource National and Local Joint Engineering Laboratory for New Petro-chemical Materials and Fine Utilization of Resources, College of Chemistry and Chemical Engineering, Hunan Normal University, Changsha, Hunan 410081, China*

email: steven.kirk@cantab.net
email: samanthajsuman@gmail.com

In this investigation we have used NG-QTAIM to fully quantity the response to the four IR-active modes of all the bonding in benzene in terms of bond-flexing, bond-torsion and bond-anharmonicity that includes the tendencies towards IR-responsivity and IR-non-responsivity. Bond-anharmonicity is found to be lacking for the C-C bonds comprising the lowest frequency mode (721.57 $cm^{-1}$) measured as the absence of bond critical point (*BCP*) sliding. Additionally, bond-flexing was absent for this mode harmonic-like variation of the profile of the variation of the wrapping (torsion) of the {***p,p'***} path-packet, referred to as the Precession K, along the conventional QTAIM bond-path, the remaining three IR-active mode possessed step-like variations in the K profiles. The presence of non-nuclear attractors was detected for the IR-active mode with frequency 1573.93 $cm^{-1}$ with C-C K profiles that most closely resemble those of the relaxed benzene. We quantified the C-H bonds in terms of bond-flexing and bond-anharmonicity and IR-responsivity and IR-non-responsivity.

## Introduction

The geometry of the bond (*bond-path*) and its response to a given normal mode is an important and overlooked aspect of the interpretation of experimental spectra. Additional oversimplifications discovered are that torsional motions occur as rigid atom-centred distortions, i.e. do not involve any bond twisting motions. Therefore, using NG-QTAIM we highlighted the disadvantages of using of group theory with mathematical models of the forms and frequencies of the molecular vibrations including using normal mode coordinate analysis and symmetry assignments[1]. The use of NG-QTAIM demonstrates the reasons for the insufficiency of current mathematical models used for analyzing experimental vibrational spectra that rely on the *ad-hoc* addition of anharmonic terms that assume linear bonding. In recent investigations we introduced a vector-based interpretation of the chemical bond within the quantum theory of atoms in molecules (NG-QTAIM) and examined the four IR-active modes of benzene and determined that the C-C and C-H bonds curve and twist thus demonstrating the weakness of assumptions about the rigidity of these short bonds[1,2]. In these investigations we plotted the $\{\boldsymbol{p},\boldsymbol{p'}\}$ and $\{\boldsymbol{q},\boldsymbol{q'}\}$ path-packets[2] and calculated the scalar lengths $\{\mathsf{H}',\mathsf{H}'^{*}\}$ and $\{\mathsf{H},\mathsf{H}^{*}\}$ respectively[1] but did not quantify the manner in which the $\{\boldsymbol{p},\boldsymbol{p'}\}$ and $\{\boldsymbol{q},\boldsymbol{q'}\}$ path-packets wrapped around the associated bond-path.

Earlier, a stress tensor trajectories $\mathsf{T}_\sigma$ in the stress tensor eigenvector projection space $\mathsf{U}_\sigma$[3,4] methodology[5] was used to explain the relative differences in the intensities of the IR-active modes of benzene[6–11] associated with changes in the dipole moment[7–9,12,13] where larger dipole moments were discovered to lead to greater IR-active mode intensities. This $\mathsf{T}_\sigma$ analysis was intended to complement the extensive studies of the vibrational modes of benzene that used semi-empirical and *ab initio* methods[14–16] and theoretical treatments on the normal coordinate treatment of benzene[6,17,18], the conventional renderings of the four infrared (IR) active modes of benzene and molecular graphs are provided in the **Supplementary Materials S1**.

The NG-QTAIM interpretation of the chemical bond as the *bond-path framework set*, denoted by $\mathsf{B}$, where $\mathsf{B} = \{\boldsymbol{p},\boldsymbol{q},\boldsymbol{r}\}$, with the consequence that for a given electronic state a bond is comprised of three 'linkages'; $\boldsymbol{p}$, $\boldsymbol{q}$ and $\boldsymbol{r}$ associated with the $\underline{\mathbf{e}}_1$, $\underline{\mathbf{e}}_2$ and $\underline{\mathbf{e}}_3$ eigenvectors, respectively. Here the $\boldsymbol{p}$ and $\boldsymbol{q}$ are 3-D paths constructed from the values of the least ($\underline{\mathbf{e}}_1$) and most ($\underline{\mathbf{e}}_2$) preferred directions of electronic charge density accumulation $\rho(\mathbf{r})$ along the conventional QTAIM bond-path, referred to within NG-QTAIM formalism as ($\boldsymbol{r}$). The directions of the $\boldsymbol{p}$-, $\boldsymbol{q}$- and $\boldsymbol{r}$-paths always remain orthogonal to each other because they are constructed from the $\underline{\mathbf{e}}_1$, $\underline{\mathbf{e}}_2$ and $\underline{\mathbf{e}}_3$ eigenvectors respectively, for in depth discussion on the construction of bond-path framework set $\mathsf{B}$ and the basic QTAIM definitions, see the **Supplementary Materials S2**.

In this investigation we seek to fully quantify for the first time the response to of the C-C *BCP* bond-path and C-H *BCP* bond-paths to the four IR-active modes in terms of the extent the $\{\boldsymbol{p},\boldsymbol{p'}\}$ and $\{\boldsymbol{q},\boldsymbol{q'}\}$ path-packets torsion or *precess* around the associated bond-path. We also seek to quantify the anharmonic response of the C-C *BCP* and C-H *BCP* to the four IR-active modes in terms of the degree of relative *BCP* sliding along the containing bond-paths. since a changing *BCP* shift in real space relative to the bond-path implies a change in chemical character due to the change of the charge density $\rho(\mathbf{r})$ distribution[19].

This will be undertaken by determining the readiness of the C-C and C-H bond-paths to respond to or resist responding to the IR irradiation. This is quantified by the extent of bond-path motion in the most facile (IR-responsivity) and least facile (IR-non-responsivity) respectively.

## 2. Theory and Methods

### *2.1 The QTAIM bond-path properties; the {**p**,**p'**} and {q,q'} path-packet precession K and K'*

Non-zero differences in the values of the BPL and GBL associated with a given *BCP* bond-path correspond to the presence of bond-path flexing. The anharmonic response of the C-C *BCP* and C-H *BCP* to the four IR-active modes is quantified in terms of the degree of relative *BCP* sliding along the containing bond-paths. This is because a changing *BCP* shift in real space relative to the bond-path implies a change in chemical character due to the change of the charge density $\rho(\mathbf{r})$ distribution[19]. To determine the presence of bond-path torsion we need to quantify the degree of torsion of the {***p***,***p'***} path-packet, a 3-D measure vector-based that is sufficient to describe bond-path torsion. The bond-path torsion may be defined as occurring about a the *BCP* or an extended region around the *BCP*, either side of the *BCP*, along the containing bond-path.

Bonds will rupture if the *BCP* and *RCP* coalesce, as this process unfolds most readily when the $\underline{\mathbf{e}}_2$ eigenvector, that indicates the most facile direction, when the $\underline{\mathbf{e}}_2$ eigenvector aligns along the *BCP→RCP* path. The maximum tendency to *avoid BCP* and *RCP* coalescence occurs when the $\underline{\mathbf{e}}_1$ eigenvector, that indicates the least facile, most resistant direction, is parallel/anti-parallel to the *BCP→RCP* path, denoted by the grey line in **Scheme 1**. We will now define the extent to which the {***p***,***p'***} path-packet, constructed from the $\underline{\mathbf{e}}_1$ eigenvector, *precesses* about the shared-shell C5-C6 *BCP* bond-path and the shared-shell C6-H12 *BCP* bond-path, see the left and right panels of **Scheme 1** respectively.

For the {***p***,***p'***} path-packet, defined by the $\underline{\mathbf{e}}_1$ eigenvector, we wish to follow the extent to which the {***p***,***p'***} path-packet precesses about the bond-path by defining the *precession* K for IR-responsivity:

$$\mathsf{K} = 1 - \cos^2\alpha, \qquad \text{where } \cos\alpha = \underline{\mathbf{e}}_1 \cdot \underline{\mathbf{u}} \qquad \text{and} \qquad 0 \leq \mathsf{K} \leq 1 \qquad \textbf{(1)}$$

Considering the extremes, K = 0, where α is defined by equation (**1**), we the maximum alignment of the *BCP→RCP* path with the $\underline{\mathbf{e}}_1$ eigenvector, the least facile direction and for K = 1 we have the maximum degree of alignment with the $\underline{\mathbf{e}}_2$ eigenvector, the most facile direction. Values of K = 0 and K = 1 also indicate bond-paths with the lowest and highest tendencies towards IR-responsivity respectively. The precession K is determined relative to the *BCP*, in either direction along the bond-path towards the nuclei at either ends of the bond-path from an arbitrarily small spacing of $\underline{\mathbf{e}}_1$ eigenvectors. If we chose the precession of the {***p***,***p'***} path-packet about the bond-path when the $\pm\underline{\mathbf{e}}_1$ eigenvector is parallel to $\underline{\mathbf{u}}$, that defines the *BCP→RCP* path, the *BCP* will have minimum facile character, i.e. IR-responsivity see **Scheme 1**. By following the variation of the precession K we can quantify the degree of facile character of a *BCP* along an

entire bond-path. For the precession of the {***q***,***q'***} path-packet, defined by the $\underline{\mathbf{e}}_2$ eigenvector, about the bond-path, $\beta = (\pi/2 - \alpha)$ and $\alpha$ is defined by equation **(2)** see **Scheme 1**, we can write an expression $K'$ for the bond-path IR-non-responsivity:

$$K' = 1 - \cos^2\beta, \qquad \text{where } \cos\beta = \underline{\mathbf{e}}_2 \cdot \underline{\mathbf{u}}, \quad \beta = (\pi/2 - \alpha) \quad \text{and} \quad 0 \leq K' \leq 1 \qquad \textbf{(2)}$$

Note, for the general case the $\underline{\mathbf{e}}_3$ eigenvector defined along the bond-path is not perpendicular to the reference direction $\underline{\mathbf{u}}$, see **Scheme 1**. For $K' = 0$ we have a maximum degree of facile character and for $K = 1$ we have the minimum degree of facile character and values of $K' = 0$ and $K' = 1$ therefore indicate bond-paths with the lowest and highest tendencies towards IR-non-responsivity respectively. We include $K'$ because for the C-H *BCP* bond-path may move out of the plane of the benzene molecule, then the $K$ and $K'$ will not necessarily be converses of each other.

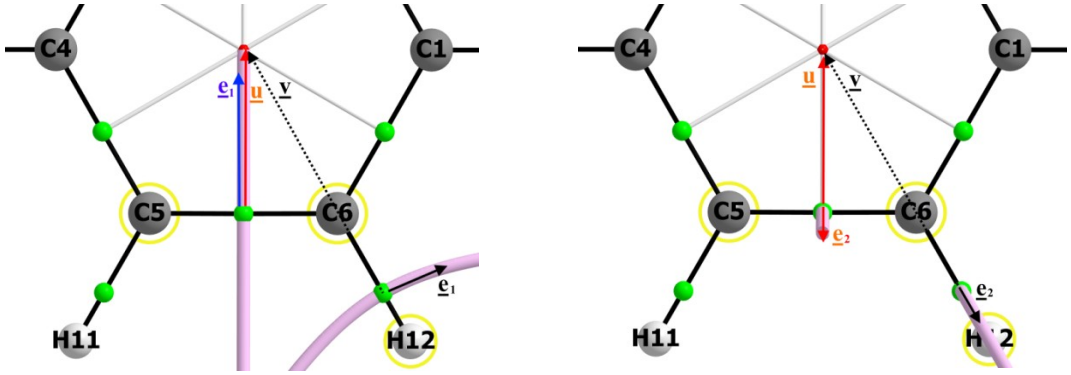


**Scheme 1.** The {***p***,***p'***} precession $K$ construction (left panel) and {***q***,***q'***} path-packet precession $K'$ (right panel) for the C5-C6 *BCP* and C6-H12 *BCP*, where the $\underline{\mathbf{u}}$ is a unit vector (red arrow) along the *BCP*→*RCP* path are denoted by the grey line. The vector $\underline{\mathbf{v}}$ is a unit vector (black arrow) defined to be aligned parallel to the normal vector of the plane of the relaxed benzene molecule. The pale magenta line indicates the interatomic surface paths (IAS) that originate at the *BCP*. The $\underline{\mathbf{e}}_1$ eigenvector (blue arrow) and $\underline{\mathbf{e}}_2$ eigenvector (magenta arrow), the ± signs of $\underline{\mathbf{e}}_1$ and $\underline{\mathbf{e}}_2$ are chosen to form the right handed orthogonal set $\{\underline{\mathbf{e}}_1, \underline{\mathbf{e}}_2, \underline{\mathbf{e}}_3\}$. The undecorated red and green spheres indicate the locations of the bond critical points (*BCP*s) and ring critical points (*RCP*s) respectively.

### 3. Computational Details

The geometry optimization and frequency calculation were undertaken with the BH and HLYP DFT functional and 6-31G(d,p) basis set with in G09 v.E.01[20]. The SCF convergence criteria were set to tighter values than the defaults, specifically to both $< 10^{-10}$ RMS change in the density matrix and $< 10^{-8}$ maximum change in the density matrix. Single-point calculations, corresponding to snapshots throughout one full cycle of each of the calculated vibrational modes, were carried out using the same functional, basis set and convergence criteria. The intermediate 'snapshot' structures were generated by an external program using the geometry-optimized structure together with the displacement directions calculated for each IR-active mode in the frequency calculation. The wave-functions produced by the snapshot single-point calculation were

subsequently analyzed using AIMAll[21] and the resulting molecular graphs were analyzed using two in-house codes, to plot the {$\boldsymbol{q}$,$\boldsymbol{q'}$} and {$\boldsymbol{p}$,$\boldsymbol{p'}$} path-packets.

## 4. Results and Discussions

The relative bond-path lengths (ΔBPL) are not significantly larger than the relative interatomic separations, referred to as the relative geometric bond lengths (ΔGBL) for the C-C *BCP* bond-paths, indicating an absence of bond-path flexing, see **Table 1**. The converse is apparent for the C-H *BCP* bond-paths and bond-path flexing is apparent from visual inspection of the molecular graphs of IR-active modes 14 and 21, see **Figure 6** and **Figure 7** respectively. Larger differences in the BPL and GBL are however apparent for the C-H *BCP* bond-path due to the facile nature of the total charge density distribution $\rho(\mathbf{r_b})$ associated with the H *NCP*. In addition, we note that the presence of values of C-H BPL < GBL is because the position of the H *NCP* does not coincide with the geometric centre of the H *NCP*. The original table of distance measures for the four infra-red (IR) active modes of benzene including the partial bond-path lengths (C-*BCP*) and (*BCP*-C/H), the bond-path lengths (BPL) and geometric bond-lengths (GBL) along with the reference values for the relaxed benzene is provided in the **Supplementary Materials S3**. The lack of significant difference between the BPL and GBL values for the C-C *BCP* bond-paths contrasts with that of the much larger range of *BCP* sliding values, quantified by the relative shifts of the C-C *BCP*s and C-H *BCP*s, see **Table 1**. From the C-C *BCP* sliding values that provide a measure of bond-anharmonicity, Δ(C-*BCP*) and Δ(*BCP*-C), we see that the order in increasingly anharmonic response of the C-C *BCP* bond-paths we have IR-active mode 5 < IR-active mode 28 < IR-active mode 14 < IR-active mode 21. The C-C *BCP* bond-paths of IR-active mode 5 can be describable as possessing effectively no or insignificant bond-anharmonicity on the basis of the Δ(C-*BCP*) and Δ(*BCP*-C) value of 0.000.

**Table 1.** The symmetry inequivalent *BCP* values of the relative partial benzene bond-path lengths Δ(C-*BCP*/*NNA*) = ΔA, Δ(*NNA*/*BCP*-C/H) = ΔB with the Δ(BPL), ΔGBL and the relative position along the bond-path that precession K jumps from K = minimum to K = 1 (–ΔQ and +ΔQ) in a.u. for the amplitudes = -1.0 and +1.0 of the infrared (IR) benzene each of the four IR-active modes are presented. The relative partial bond path lengths Δ(C-*BCP*/*NNA*) and Δ(*BCP*/*NNA*-C/H) were calculated by subtracting off the relaxed benzene values. For the relaxed benzene –Q and +Q values are -0.700 and 0.700 respectively, see the **Table S3** of the **Supplementary Materials S3**. The four infrared (IR) active normal modes of benzene are ordered according to their increasing frequency, corresponding to 721.57 $cm^{-1}$ (mode 5), 1097.69 $cm^{-1}$ (mode 14), 1573.93 $cm^{-1}$ (mode 21) and 3298.32 $cm^{-1}$ (mode 28) respectively. For IR-active mode 21 the '*' indicates the presence of a non-nuclear attractor (*NNA*). In IR-active mode 28 the C-C *BCP* bond-paths that are unresponsive are indicated by '**U**'. The values of ±ΔQ for mode 5 were estimated as half way up the slope of the non-step-like variation in the K profile.

| | | -1.0 | | | +1.0 | |
|---|---|---|---|---|---|---|
| *BCP* | (ΔA, ΔB) | ΔBPL(ΔGBL) | (+ΔQ,- ΔQ) | (ΔA, ΔB) | ΔBPL(ΔGBL) | (+ΔQ,- ΔQ) |
| | | | *IR-active mode 5* | | | |
| C1-C2 | (0.000, 0.000) | 0.000(0.000) | (0.037, -0.037) | (0.000, 0.000) | 0.000(0.000) | (0.037, -0.037) |
| C1-H7 | (0.116, 0.047) | 0.169(0.163) | (---, ---) | (0.116, 0.047) | 0.169(0.163) | (---, ---) |
| | | | *IR-active mode 14* | | | |
| C1-C2 | (-0.151, -0.151) | -0.302(-0.302) | (-0.071, 0.071) | (0.152, 0.152) | 0.303(0.303) | (0.175, -0.175) |
| C2-C3 | (0.085, 0.101) | 0.185(0.184) | (-0.075, 0.075) | (0.085, 0.101) | 0.185(0.184) | (0.050, -0.150) |
| C3-C4 | (-0.065, -0.090) | -0.154(-0.154) | (0.150, -0.050) | (-0.065,-0.090) | -0.154(-0.154) | (-0.075, -0.075) |
| C4-C5 | (0.152, 0.152) | 0.303(0.303) | (0.175, -0.175) | (-0.151,-0.151) | -0.302(-0.302) | (-0.071, 0.071) |
| C1-H7 | (0.002, 0.030) | 0.034(0.031) | (---, ---) | (0.071, -0.004) | 0.069(0.067) | (---, ---) |
| C3-H9 | (0.134, 0.052) | 0.195(0.185) | (---, ---) | (0.134, 0.052) | 0.195(0.185) | (---, ---) |
| C5-H11 | (0.027, -0.006) | 0.069(0.067) | (---, ---) | (0.002, 0.030) | 0.034(0.031) | (---, ---) |
| | | | *IR-active mode 21* | | | |
| C1-C2 | (0.208, 0.208) | 0.416(0.416) | (0.000, 0.000) | (-0.208, -0.208)* | -0.415(-0.415) | (-0.028, 0.028) |
| C2-C3 | (0.187, 0.026) | 0.215(0.213) | (-0.150, -0.175) | (-0.177, 0.012) | -0.164(-0.165) | (0.150, 0.200) |
| C3-C4 | (0.012, -0.177) | -0.164(-0.165) | (-0.200, -0.150) | (0.026, 0.187) | 0.215(0.213) | (0.175, 0.150) |
| C4-C5 | (-0.208, -0.208)* | -0.415(-0.415) | (-0.028, 0.028) | (0.208, 0.208) | 0.416(0.416) | (0.000, 0.000) |
| C1-H7 | (0.112, 0.027) | 0.145(0.138) | (---, ---) | (0.048, 0.021) | 0.074(0.067) | (---, ---) |
| C3-H9 | (0.286, 0.102) | 0.405(0.381) | (---, ---) | (0.286, 0.102) | 0.405(0.381) | (---, ---) |
| C5-H11 | (0.009, 0.021) | 0.074(0.067) | (---, ---) | (0.112, 0.027) | 0.145(0.138) | (---, ---) |
| | | | *IR-active mode 28* | | | |
| C1-C2 | (-0.037, -0.037) | -0.074(-0.075) | (**U**, **U**) | (0.038, 0.038) | 0.078(0.076) | (-0.225, 0.225) |
| C2-C3 | (0.014, -0.059) | -0.044(-0.045) | (-0.050, **U**) | (0.027, 0.021) | 0.049(0.048) | (0.000, 0.225) |
| C3-C4 | (0.021, 0.027) | 0.049(0.048) | (-0.225, 0.000) | (-0.059, 0.014) | -0.044(-0.045) | (**U**, 0.050) |
| C4-C5 | (0.152, 0.152) | 0.303(0.303) | (-0.225, 0.225) | (0.019, 0.019) | 0.038(0.038) | (**U**, **U**) |
| C1-H7 | (0.639, 0.386) | 1.047(1.024) | (---, ---) | (-0.648,-0.377) | -1.042(-1.024) | (---, ---) |
| C3-H9 | (0.009, -0.008) | 0.000(0.000) | (---, ---) | (0.009, -0.008) | 0.000(0.000) | (---, ---) |
| C5-H11 | (-0.648, -0.377) | -1.042(-1.024) | (---, ---) | (0.639, 0.386) | 1.047(1.024) | (---, ---) |

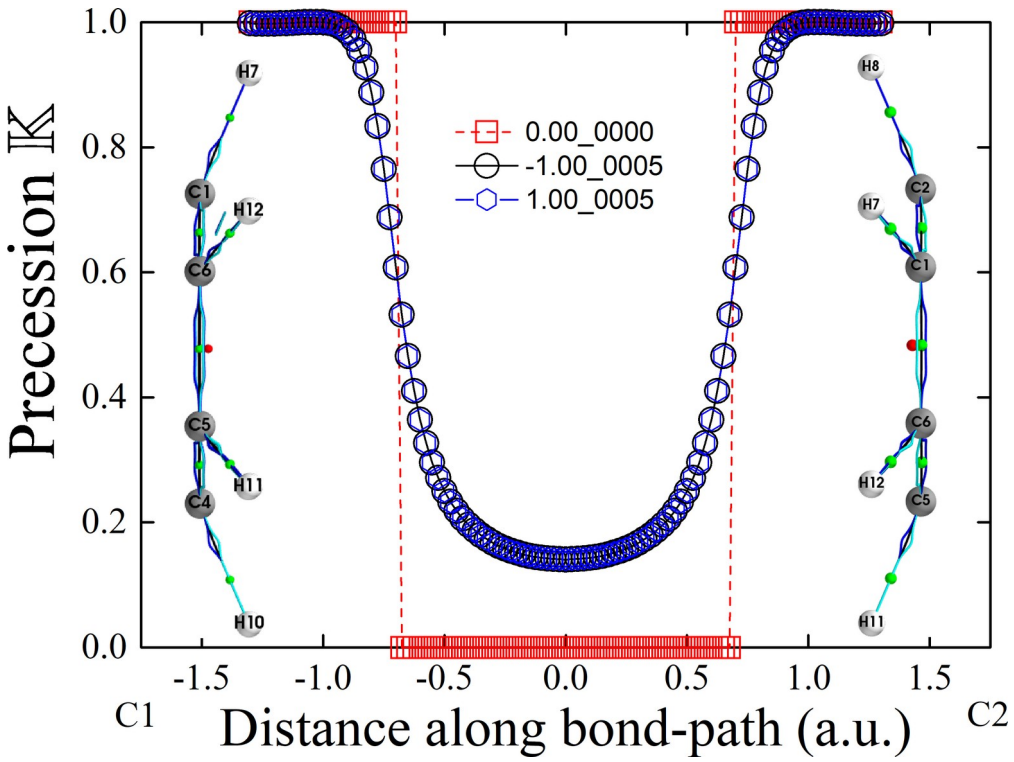


**Figure 1.** The variation of the precession K along the C-C *BCP* bond-paths of the benzene IR-active mode 5 for the amplitudes of vibration -1.0 (black), 0.0 (red) and +1.0(blue). The {***p***,***p'***} path-packets are superimposed onto the molecular graph and shown on the insets for amplitude -1.0 (left) and +1.0 (right). Bond critical points (*BCP*s) are located at a distance = 0.0 a.u along the bond-path, the ring critical point (*RCP*) is visible as the green sphere located outside of the plane of the benzene ring, see the caption of **Table 1** for further details.

For the C-C *BCP* bond-paths the K and K′ are the converse of one another so we provide the K′ plots in the **Supplementary Materials S4**. The values of the relative position along the bond-path that the values of the precession K jumps from K = minimum to K = 1 (–ΔQ and +ΔQ) for the C-C *BCP* bond-paths are not correlated with the *BCP* shifts, e.g. see the entries for the C1-C2 *BCP* for the IR-active mode 14 presented in **Table 1**. For amplitudes ±1.0 the K (and K′) profiles of the C-C *BCP* bond-paths of IR-active mode 5 possess a harmonic-like morphology, explainable by the non-planar molecular graph of IR-active mode 5, where the *RCP* is visible the side view, see **Figure 1**. Conversely, the relaxed benzene and the other three IR-active modes possess step-like K (and K′) profiles for the C-C *BCP* bond-paths and planar molecular graphs, see **Figures 2-4**. Mode 14 is the only mode where the values of |ΔQ| are the same for the amplitudes ±1.0, although the precession K (and K′) profiles are not symmetrical, see **Figure 2**. For mode 21, the presence of the non-nuclear attractors (*NNA*s)[22,23] for both the C1-C2 *BCP* bond-path (amplitude = +1.0) and C4-C5 *BCP* (amplitude = -1.0) bond-path is noted and results in values of ±ΔQ comparable to the relaxed benzene and symmetrical precession K (and K′) profiles, see **Figure 3**. Conversely, for mode 21 the bond-paths lacking an *NNA* possess a greater range of the values of ±ΔQ and asymmetrical precession K (and K′) profiles.

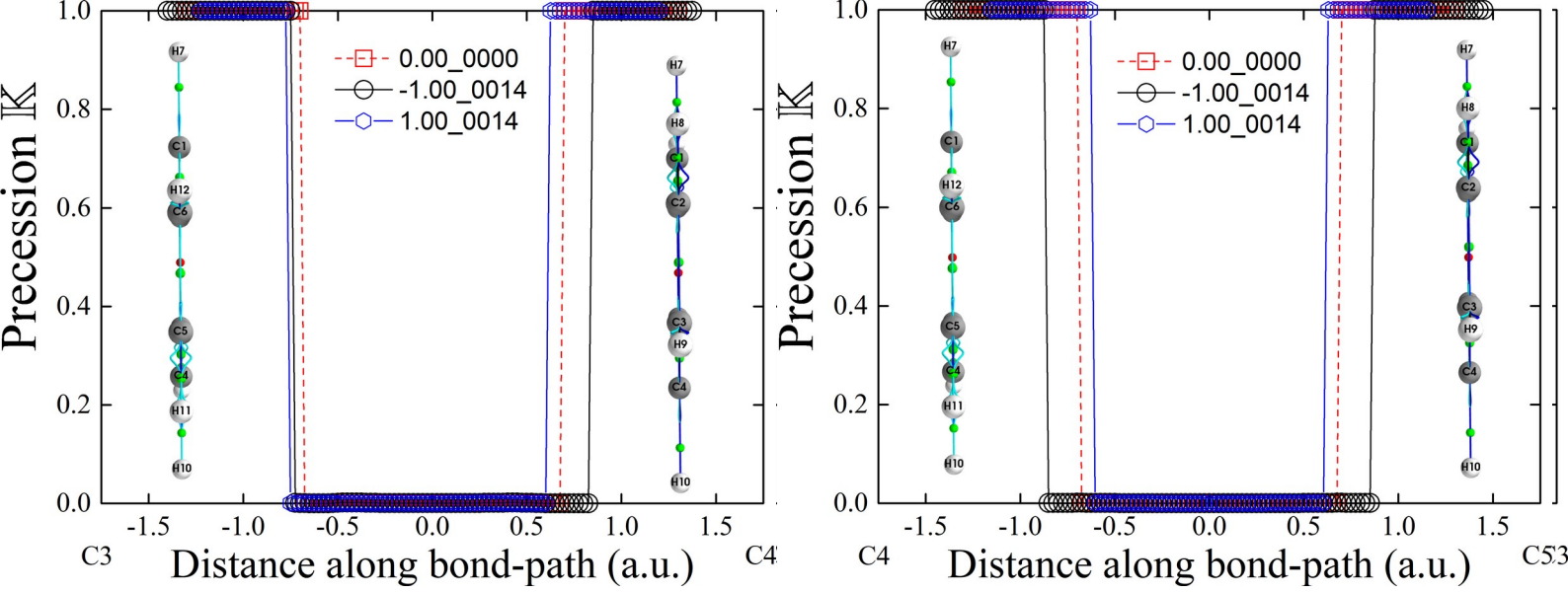


**Figure 2.** The variation of the precession K along the C-C *BCP* bond-paths of the benzene IR-active mode 14, see the caption of **Figure 1** for further details.

Lower/higher values of ±Q determined for the precession K indicate that the associated C-C *BCP* bond-path is more/less IR-responsive. A complete lack of IR-responsivity is seen e.g. for the C1-C2 *BCP* bond-path of mode 28 with amplitude = -1.0 and is indicated by the initial **U** (non-responsive), see **Table 1 and Figure 4**.

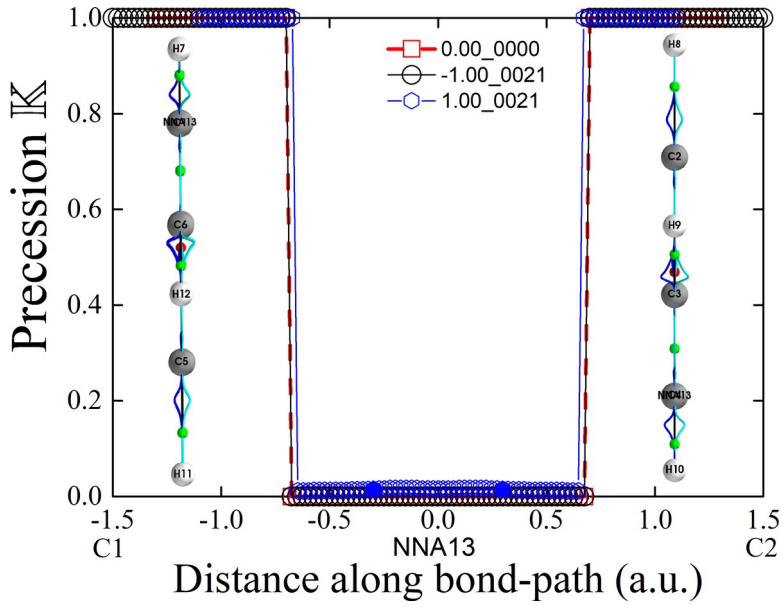


(a)

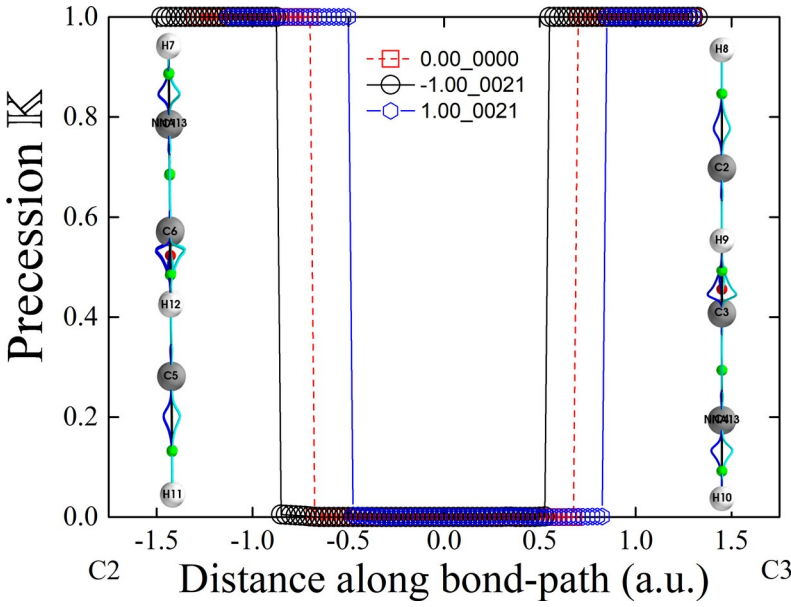


(b)

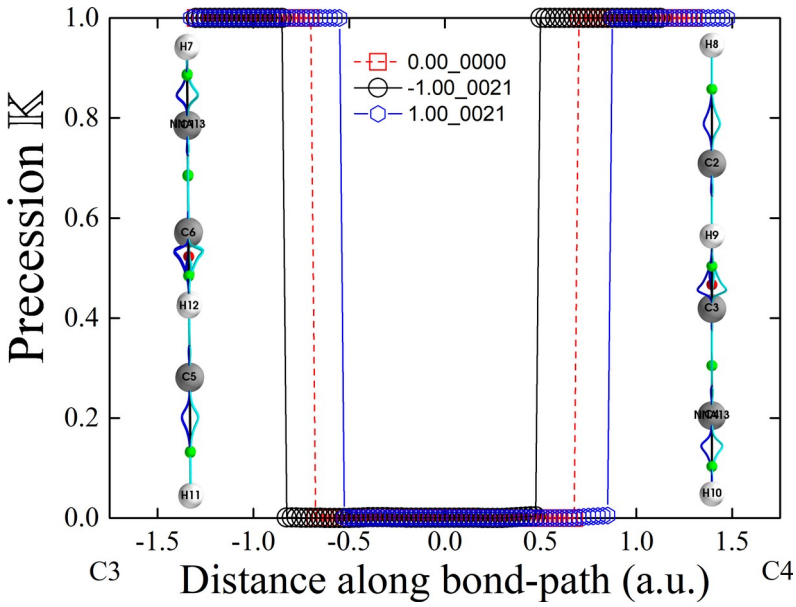


(c)

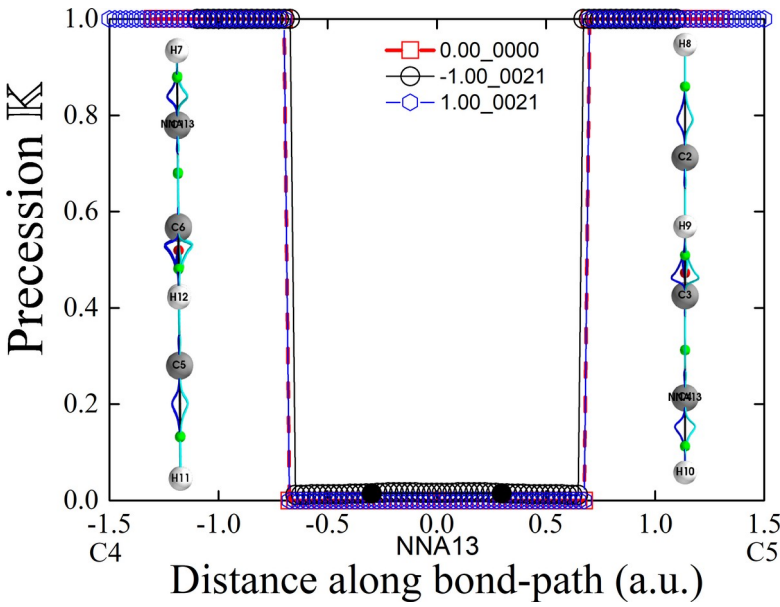


(d)

**Figure 3.** The variation of the precession K along the C-C *BCP* bond-paths of the benzene IR-active mode 21, see the caption of **Figure 1** for further details. Note the presence of non-nuclear attractors (*NNA*s) for the C1-C2 *BCP* bond-path (blue spheres) and C4-C5 *BCP* bond-path (black spheres).

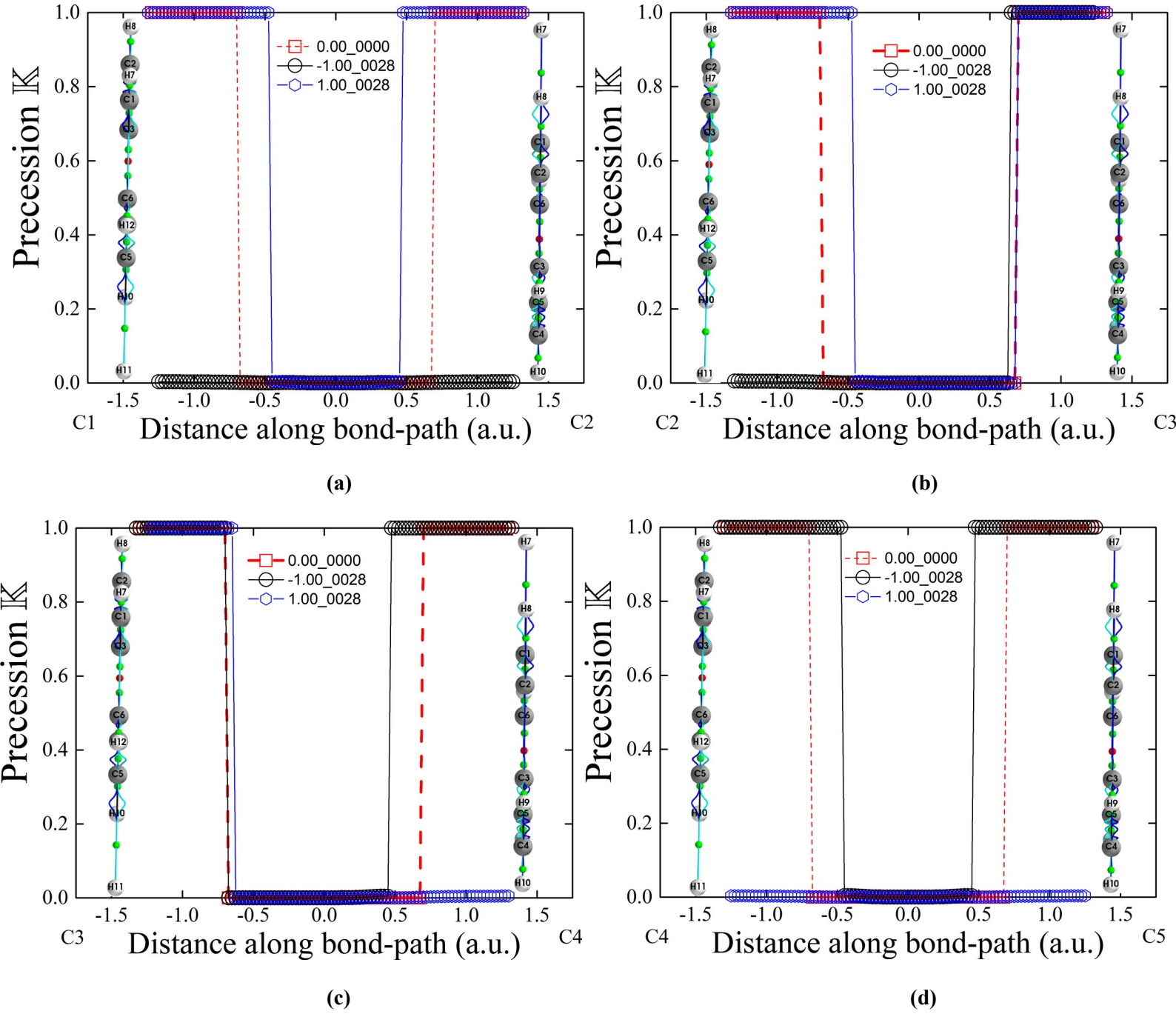


**Figure 4.** The variation of the precession K along the C-C *BCP* bond-paths of the benzene IR-active mode 28, see the caption of **Figure 1** for further details.

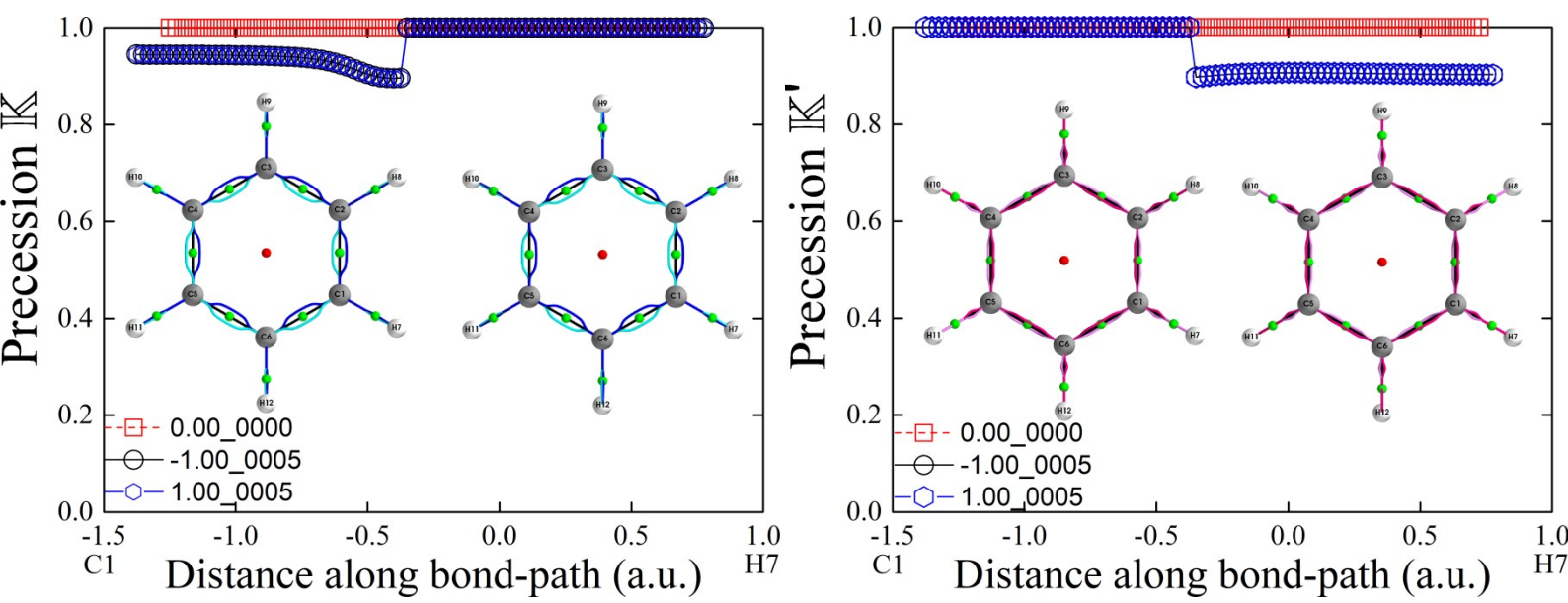


**Figure 5.** The precession K and K′ values for the C-H *BCP* bond-paths of the benzene IR-active mode 5 for the amplitudes of vibration -1.0 (black), 0.0 (red) and +1.0(blue). The variation of the precession K with inset {***p***,***p'***} path-packets (left panel) and K′ with inset {***q***,***q'***} (right panel) along the C-C *BCP* bond-paths of the relaxed benzene. Bond critical points (*BCP*s) are located at a distance = 0.0 a.u along the bond-path.

The converse relation between K and K′ does not hold for the C-H *BCP* bond-paths, see **Figures 5-8** and the theory section. Values of the Precession K = 0 and K = 1 indicate bond-paths with the lowest and highest tendencies towards IR-responsivity and this explains why the K values for facile C-H *BCP* bond-path remain close to K = 1, exactly 1.0 for the C-H *BCP* bond-path of the relaxed benzene with some exception for IR-active mode 21, see **Figures 5-8**. The C-H *BCP* bond-paths of IR-active mode 28 contain the lowest (C3-H9 *BCP*) and highest (C1-H7 *BCP*) degree of bond-anharmonicity as well as bond-flexing.

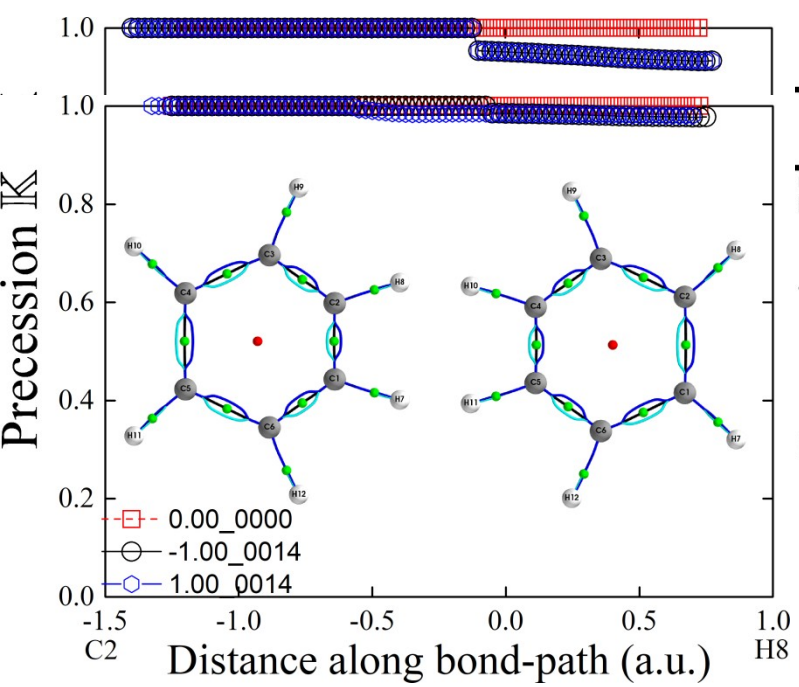
Precession 𝕂
1.0
0.8
0.6
0.4
0.2
0.0
0.00_0000
-1.00_0014
1.00_0014
-1.5
-1.0
-0.5
0.0
0.5
1.0
C2
H8
Distance along bond-path (a.u.)

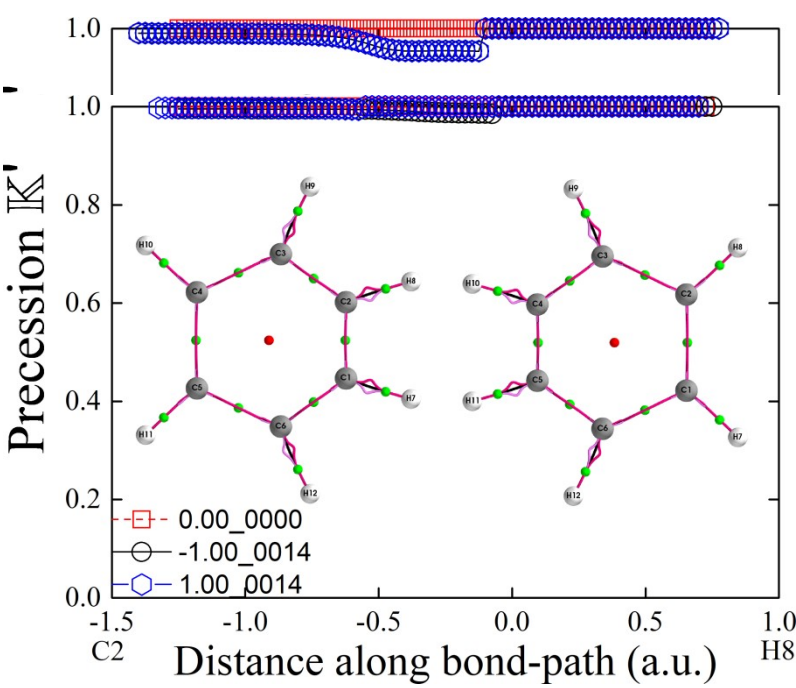
Precession 𝕂'
1.0
0.8
0.6
0.4
0.2
0.0
0.00_0000
-1.00_0014
1.00_0014
-1.5
-1.0
-0.5
0.0
0.5
1.0
C2
H8
Distance along bond-path (a.u.)

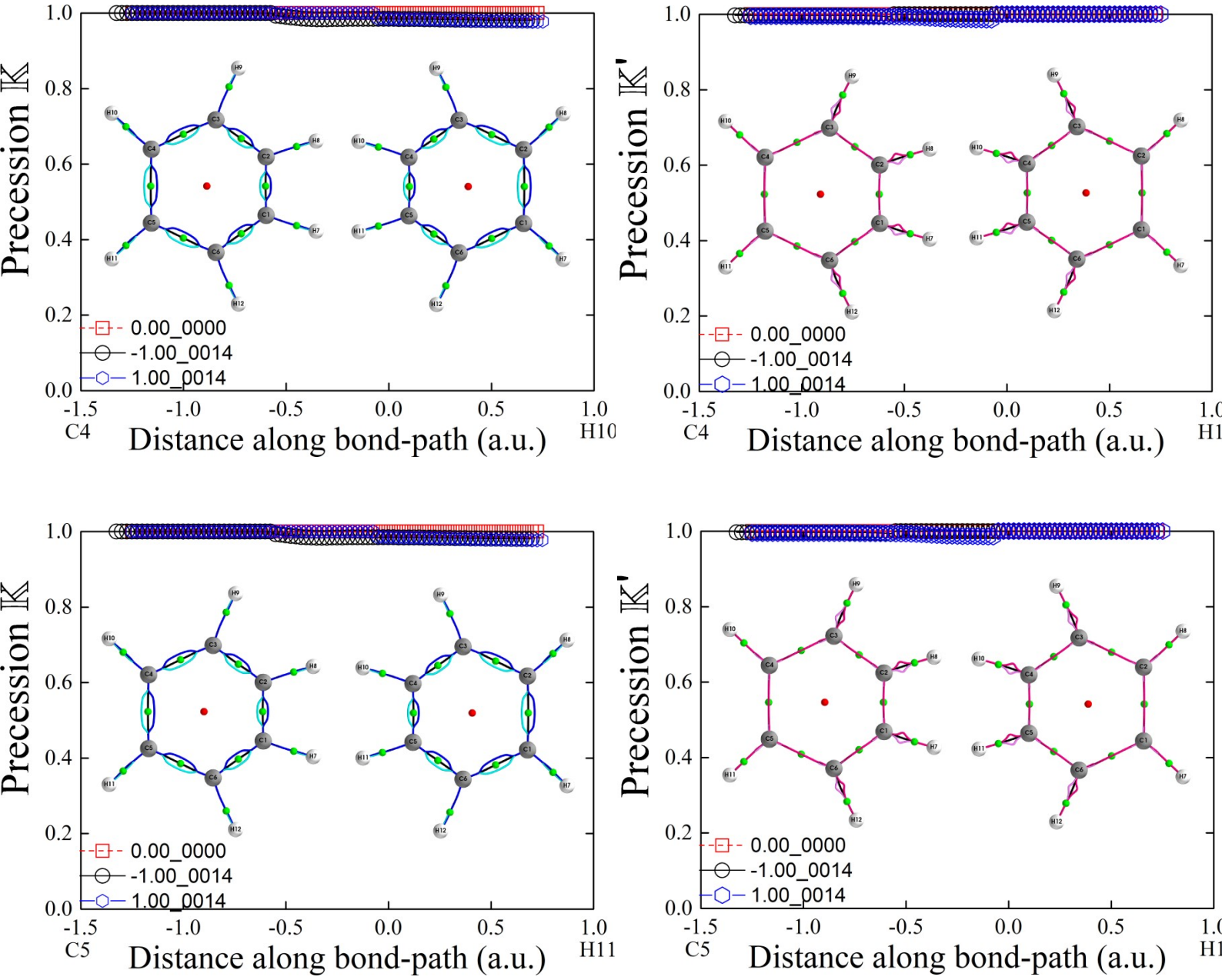


**Figure 6.** The precession K and K′ values for the C-H *BCP* bond-paths of the benzene infrared IR-active mode 14, see the caption of **Figure 5** for further details.

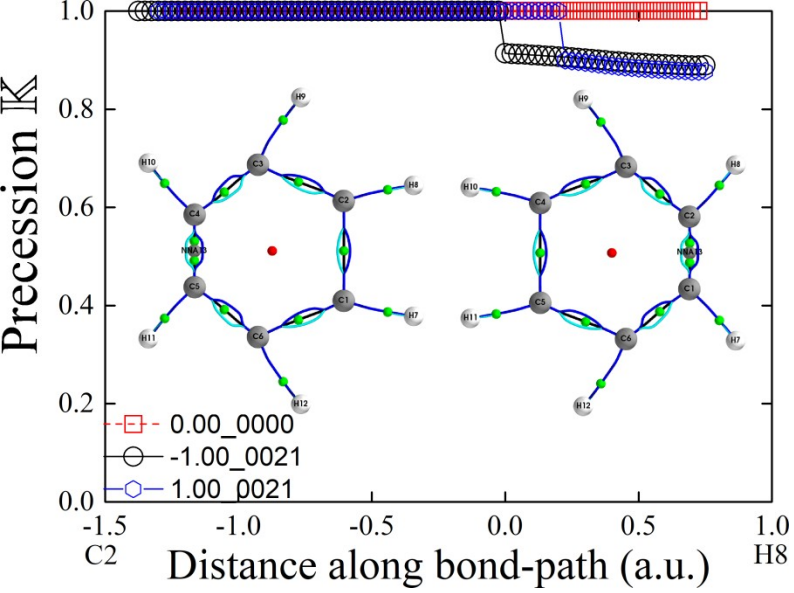
Precession 𝕂
1.0
0.8
0.6
0.4
0.2
0.0
0.00_0000
-1.00_0021
1.00_0021
-1.5
-1.0
-0.5
0.0
0.5
1.0
C2
H8
Distance along bond-path (a.u.)

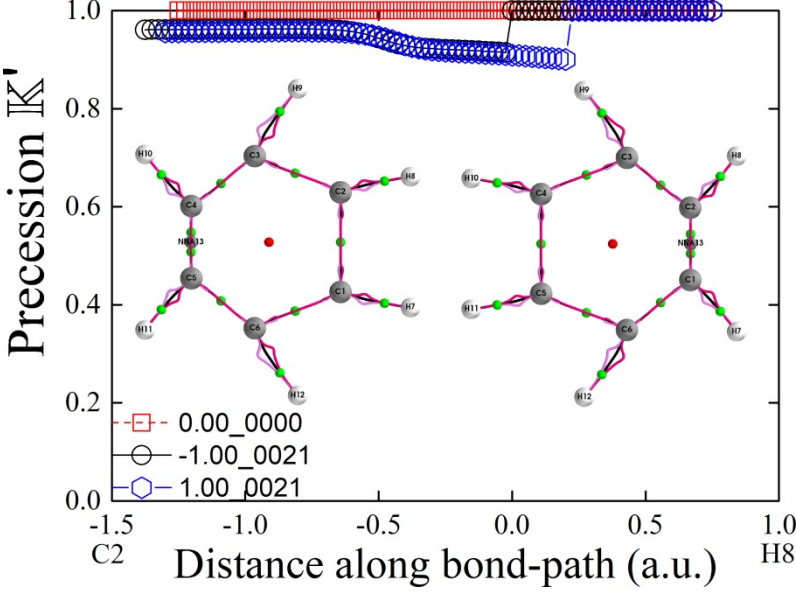
Precession 𝕂'
1.0
0.8
0.6
0.4
0.2
0.0
0.00_0000
-1.00_0021
1.00_0021
-1.5
-1.0
-0.5
0.0
0.5
1.0
C2
H8
Distance along bond-path (a.u.)

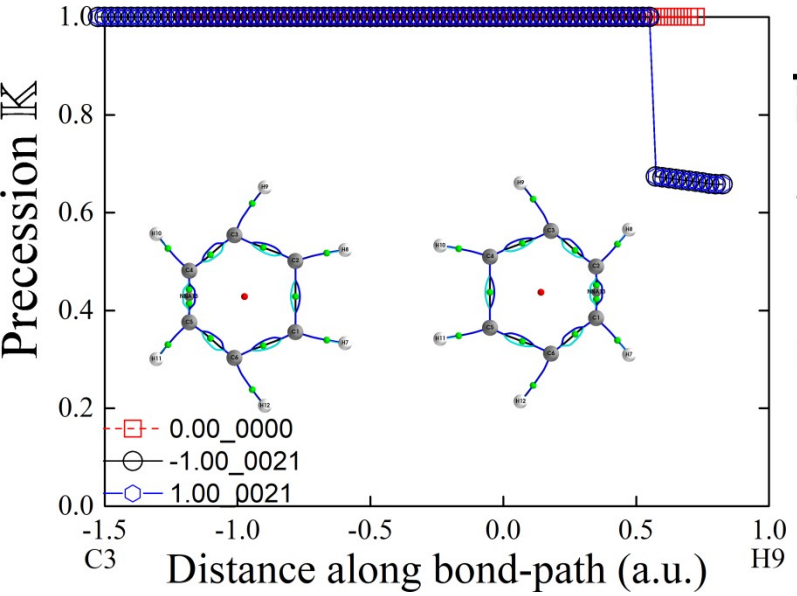
Precession 𝕂
1.0
0.8
0.6
0.4
0.2
0.0
0.00_0000
-1.00_0021
1.00_0021
-1.5
-1.0
-0.5
0.0
0.5
1.0
C3
H9
Distance along bond-path (a.u.)

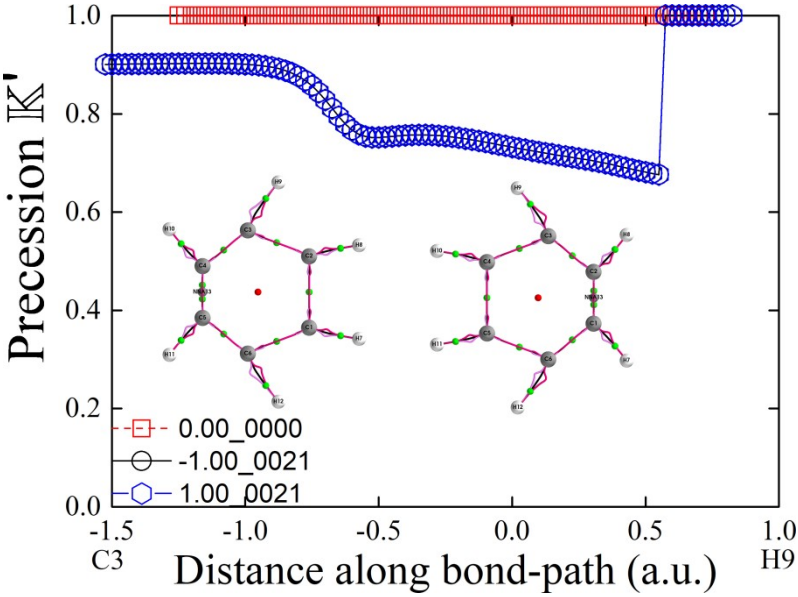
Precession 𝕂'
1.0
0.8
0.6
0.4
0.2
0.0
0.00_0000
-1.00_0021
1.00_0021
-1.5
-1.0
-0.5
0.0
0.5
1.0
C3
H9
Distance along bond-path (a.u.)

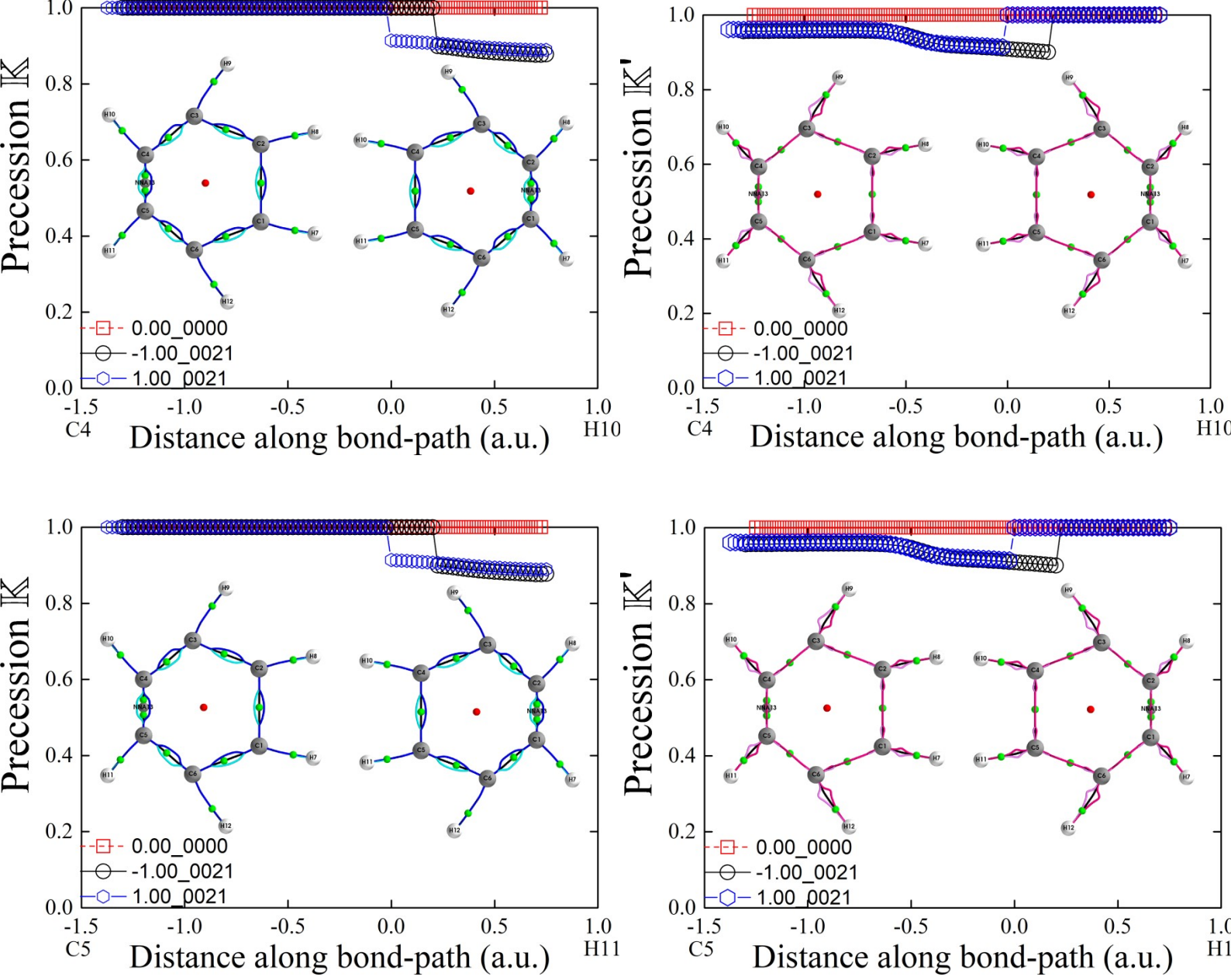


**Figure 7.** The precession K and K′ values for the C-H *BCP* bond-paths of the benzene IR-active mode 21, see the caption of **Figure 5** for further details.

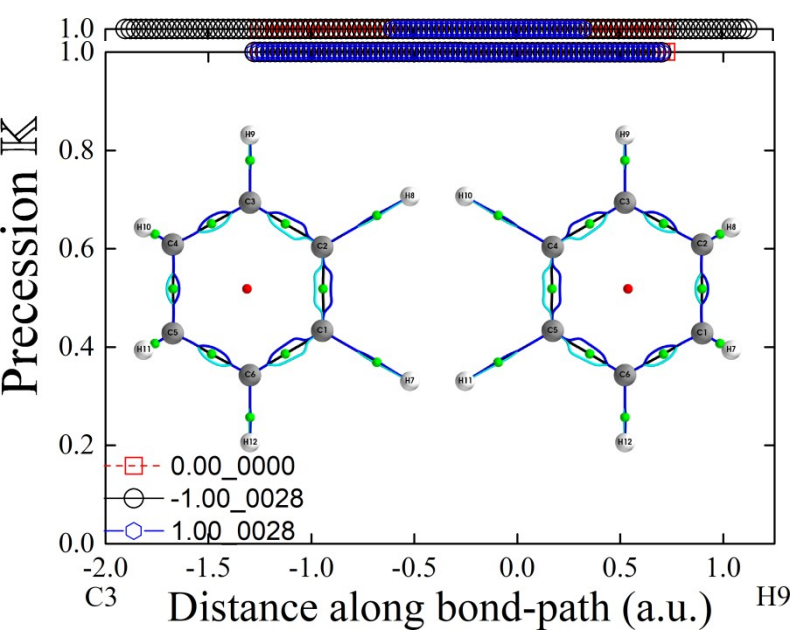
Precession 𝕂
1.0
0.8
0.6
0.4
0.2
0.0
0.00_0000
-1.00_0028
1.00_0028
-2.0
-1.5
-1.0
-0.5
0.0
0.5
1.0
C3
Distance along bond-path (a.u.)
H9

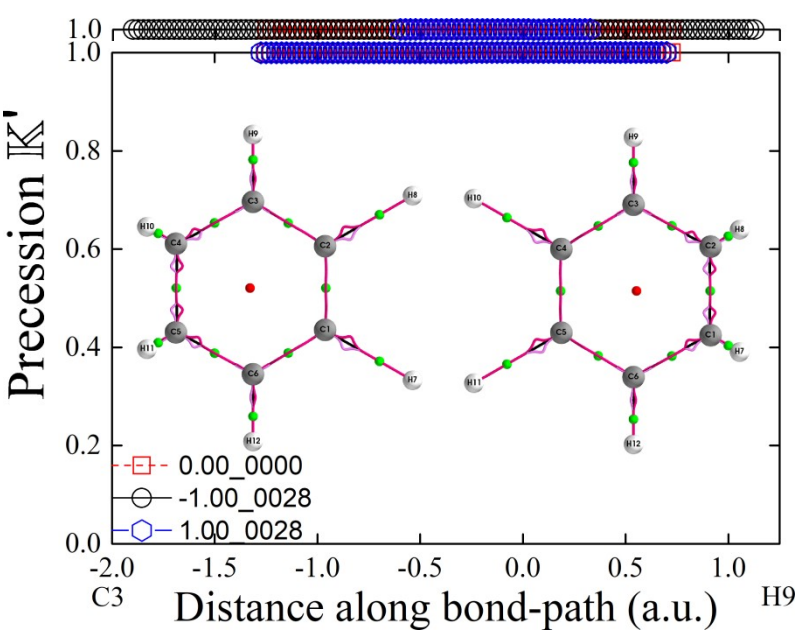
Precession 𝕂'
1.0
0.8
0.6
0.4
0.2
0.0
0.00_0000
-1.00_0028
1.00_0028
-2.0
-1.5
-1.0
-0.5
0.0
0.5
1.0
C3
Distance along bond-path (a.u.)
H9

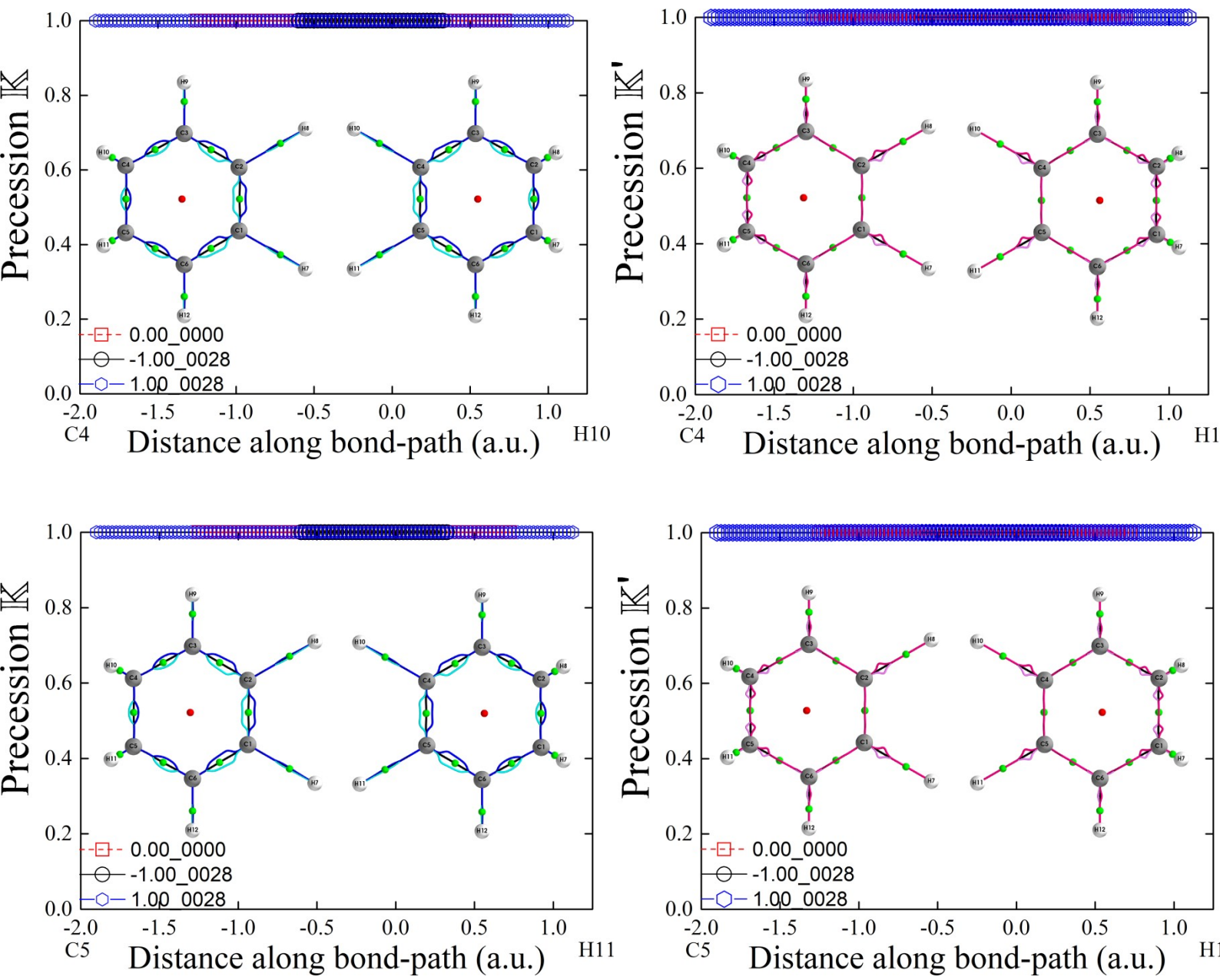


**Figure 8.** The precession K and K′ values for the C-H *BCP* bond-paths of the benzene IR-active mode 28, see the caption of **Figure 5** for further details.

## Conclusions

In this investigation we have used NG-QTAIM to complete the quantification of the changes in 3-D that occur along a bond-path. We have applied this complete analysis to quantify the four IR-active modes of benzene in terms of the bond-flexing, bond-torsion and bond-anharmonicity that includes the tendencies towards IR-responsivity and IR-non-responsivity. The precessions {K,K′} quantify the degree the wrapping of the {$\boldsymbol{p}$,$\boldsymbol{p'}$} path-packet and is constructed from the $\underline{\mathbf{e}}_1$ eigenvector and {$\boldsymbol{q}$,$\boldsymbol{q'}$} path-packet is constructed from the $\underline{\mathbf{e}}_2$ eigenvector. The anharmonicity is determined from the relative *BCP* shifts that quantify the sliding of $\underline{\mathbf{e}}_3$, defined at the *BCP*. The orthogonality of {$\underline{\mathbf{e}}_1$, $\underline{\mathbf{e}}_2$, $\underline{\mathbf{e}}_3$} explains, for the C-C *BCP* bond-paths, the lack of dependency of the relative positions along the bond-path ±ΔQ of the jumps in K and the *BCP* shifts, so $\underline{\mathbf{e}}_3$ will move with the *BCP* independently of the {$\boldsymbol{p}$,$\boldsymbol{p'}$} and {$\boldsymbol{q}$,$\boldsymbol{q'}$} path-packets constructed from the $\underline{\mathbf{e}}_1$ and $\underline{\mathbf{e}}_2$ respectively.

The harmonic K profile seen for mode 5 along with the zero values for the relative C-C *BCP* shifts indicates that the *BCP* shift is a good indicator of anharmonicity. This can be seen from the result that non-zero *BCP* shifts corresponds to a change in chemical character due to the change of the charge density $\rho(\mathbf{r})$ distribution[19], therefore for mode 5 we have no change in chemical character. This is consistent with mode 5 being the only mode where the benzene molecular graph is non-planar: the C-H *BCP* bond-paths flex out the plane of the benzene ring that results in the ring critical point (*RCP*) being located outside of the $C_6$ ring. Additionally, the minimum value of the C-C bond-path K profile of mode 5 is non-zero, unlike the three other IR-active modes. This indicates a lower degree of shared-shell character, lower IR-responsivity and a more pliable, less stiff response of the bond-path.

The presence of non-nuclear attractors (*NNA*s) in mode 21 disrupts the measurement of the relative C-C *BCP* shifts because there are now two *BCP*s and an *NNA* located along the C-C bond-path that renders the topology non-equivalent to that of the C-C bond-path of the relaxed benzene. The affect however, of the *NNA*s on the torsion of the bond-path can still be determined by examination of the precession K profile and the relative positions along the bond-path $\pm\Delta Q$ of the jumps in K. The presence of the *NNA*s corresponds to K profiles and values of $\pm\Delta Q$ that are the most similar to the relaxed benzene.

The C-H *BCP* bond-path K profiles values consistently indicate high IR-responsivity on the basis of the K profiles values being non-zero and much closer to K = 1.0 than is the case for the C-H *BCP* bond-path K profiles. The C-H *BCP* bond-paths therefore are more flexible and pliable than the C-C *BCP* bond-paths. The response {K,K′} of the C-H *BCP* bond-paths to mode 28 demonstrates large deviations from the high/high IR-responsivity/non-responsivity K = 1.0/ K′ = 1.0. Conversely the corresponding K profiles of the C-C bond-paths of mode 28 maintain K = 0.0, referred to as unresponsive (**U**) and therefore possess the stiffest C-C bonds.

**Acknowledgements**

The National Natural Science Foundation of China is gratefully acknowledged, project approval number: 21673071. The One Hundred Talents Foundation of Hunan Province is also gratefully acknowledged for the support of S.J. and S.R.K.

**References**

1. W. J. Huang, A. Azizi, T. Xu, S. R. Kirk and S. Jenkins, *Int. J. Quantum Chem.*, **2018**, 118, e25698.
2. W. J. Huang, T. Xu, S. R. Kirk and S. Jenkins, *Chem. Phys. Lett.*, **2018**, 710, 31–38.
3. T. Xu, J. Farrell, R. Momen, A. Azizi, S. R. Kirk, S. Jenkins and D. J. Wales, *Chem. Phys. Lett.*, **2017**, 667, 25–31.

4. H. Guo, A. Morales-Bayuelo, T. Xu, R. Momen, L. Wang, P. Yang, S. R. Kirk and S. Jenkins, *J. Comput. Chem.*, **2016**, 37, 2722–2733.
5. M. X. Hu, T. Xu, R. Momen, A. Azizi, S. R. Kirk and S. Jenkins, *Chem. Phys. Lett.*, **2017**, 677, 156–161.
6. E. B. Wilson, *Phys. Rev.*, **1934**, 45, 706–714.
7. M. Margoshes and V. A. Fassel, *Spectrochim. Acta*, **1955**, 7, 14–24.
8. R. G. Satink, H. Piest, G. von Helden and G. Meijer, *J. Chem. Phys.*, **1999**, 111, 10750–10753.
9. A. R. H. Cole and A. J. Michell, *Spectrochim. Acta*, **1964**, 20, 739–746.
10. W Thomson, *Theory of Vibration with Applications*, Nelson Thornes Ltd, **2018**.
11. G Varsanyi, *Vibrational Spectra of Benzene Derivatives*, Elsevier, **2012**.
12. R. P. Bell, H. W. Thompson and E. E. Vago, *Proc. R. Soc. Lond. Ser. Math. Phys. Sci.*, **1948**, 192, 498–507.
13. Mulliken, R. S., *Mulliken, R. S. Spectroscopy, Molecular Orbitals, and Chemical Bonding. Science 157, 13–24*, **1967**.
14. M. Alcolea Palafox, *Int. J. Quantum Chem.*, **2000**, 77, 661–684.
15. M. Goeppert‐Mayer and A. L. Sklar, *J. Chem. Phys.*, **1938**, 6, 645–652.
16. N. C. Handy, C. W. Murray and R. D. Amos, *J. Phys. Chem.*, **1993**, 97, 4392–4396.
17. Shafiee, G. H., Sadjadi, S. A., Najafpour, J., & Shafice, H., *J Phys Theor Chem*, **2009**, 6(2), 1–6.
18. R. C. Lord and D. H. Andrews, *J. Phys. Chem.*, **1937**, 41, 149–158.
19. T. Tian, T. Xu, S. R. Kirk, I. T. Rongde, Y. B. Tan, S. Manzhos, Y. Shigeta and S. Jenkins, *Phys. Chem. Chem. Phys.*, **2020**, 22, 2509–2520.
20. M. J. W. T. Frisch H. B. Schlegel, G. E. Scuseria, M. A. Robb, J. R. Cheeseman, G. Scalmani, V. Barone, B. Mennucci, G. A. Petersson, H. Nakatsuji, M. Caricato, X. Li, H. P. Hratchian, A. F. Izmaylov, J. Bloino, G. Zheng, J. L. Sonnenberg, *Gaussian 09, Revision E.01*, Gaussian, Inc., Wallingford, CT, USA, **2009**.
21. T. A. Keith, *AIMAll, Revision 17.01.25*, TK Gristmill Software, Overland Park KS, USA, **2017**.
22. A. Azizi, R. Momen, S. R. Kirk and S. Jenkins, *Phys. Chem. Chem. Phys.*, **2020**, 22, 864–877.
23. A. Azizi, R. Momen, T. Xu, S. R. Kirk and S. Jenkins, *Phys. Chem. Chem. Phys.*, **2018**, 20, 24695–24707.